Flood Analysis and Mapping Using Sentinel Imagery: A Case Study from Tarsus Plain, Turkey

R. Cuneyt Erenoglu[1]
https://orcid.org/0000-0002-8212-8379

Enis Arslan[2*]
https://orcid.org/0000-0002-2609-3925

[1] C.O.M.U, Faculty of Engineering, Department of Geomatics Engineering, 17100, Canakkale
[2] Çukurova University, Faculty of Engineering, Department of Computer Engineering, 01380, Adana

*Sorumlu yazar: enisarslan@gmail.com

Abstract

Floods are natural disasters that corrupt vegetation, cause loss of lives, and harm economies. There are many cases floods originate, sometimes natural, sometimes man-made. The use of agricultural fields unconsciously, land cover modifications, incorrect city planning can be listed as unnatural reasons. Modeling and mapping the floods, real-time monitoring with satellite are cost-efficient ways of decreasing the causes of floods and helping the authorities to give the exact decisions during or after the event.

Synthetic-aperture radar (SAR) satellite imagery helps in monitoring disasters like flooding. The all-weather operating capability provides cloud-free day and night imagery, even in the worst weather conditions. In this paper, Sentinel-1 satellite imagery provided by European Space Agency (ESA) is used to investigate the flood event that happened in January 2020 in the Tarsus agricultural field (West Cukurova Region) of Mersin, Turkey. Sentinel-1 imagery for the nearest dates is collected, pre-processed, and thresholded with Otsu's method and a flood map is obtained. Sentinel-2 satellite imagery for the same study area is used to verify the Sentinel-1 output composite. Spectral indices are applied on Sentinel-2 composite and classification is done with Random Forests, CART, Support Vector Machine (SVM) and Naive Bayes algorithms. Random Forest and SVM algorithms provided the best classification result. Finally, Sentinel-1 and Sentinel-2 products are overlaid as change management.

Key Words: Spectral Indices, Otsu thresholding, Google Earth Engine, Remote Sensing, Classification

Sentinel-1 Uydusu Kullanılarak Sel Analizi ve Haritalanması : Tarsus Ovası Çalışması

Özet

Seller, bitki örtüsünü bozan, can kayıplarına neden olan ve ekonomilere zaran veren doğal afetlerdir. Bazen doğal bazen insan kaynaklı olacak şekilde selleri oluşturan pekçok sebep vardır. Doğal olmayan nedenlere tarım alanlarının bilinçsizce kullanılması, arazi örtüsü değişiklikleri, yanlış şehir planlaması gibi örnekler verilebilir. Selleri modellemek ve haritalamak, uydu ile gerçek zamanlı izleme, sellerin nedenlerini azaltmanın uygun maliyetli yollarıdır ve yetkililerin olay sırasında veya sonrasında doğru kararlar verebilmelerine yardımcı olmaktadır.

Sentetik açıklıklı radar (SAR) uydu görüntüleri, sel gibi afetlerin izlenmesine yardımcı olmaktadır. Tüm hava koşullarında çalışma özelliği, en kötü hava koşullarında bile bulutsuz gündüz ve gece görüntüleri sağlamaktadır. Bu makalede, Avrupa Uzay Ajansı (ESA) tarafından sağlanan Sentinel-1 uydu görüntüleri, Mersin ili Tarsus tarım alanlarında (Batı Çukurova Bölgesi) 2020 Ocak ayında meydana gelen sel olayını araştırmak için kullanılmıştır. En yakın tarihlere ait Sentinel-1 görüntüleri ön işlemden geçirilerek Otsu yöntemiyle eşiklenmiş ve taşkın haritası elde edilmiştir. Sentinel-1 çıktı kompozitini doğrulamak için aynı çalışma alanı için Sentinel-2 uydu görüntüleri kullanılmıştır. Spektral indisler Sentinel-2 kompoziti üzerine uygulanmış ve Random Forests, CART, Support Vector Machine (SVM) ve Naive Bayes algoritmaları ile sınıflandırma yapılmıştır. Random Forest ve SVM algoritmaları en iyi sınıflandırma sonucunu sağlamıştır. Son olarak, Sentinel-1 ve Sentinel-2 ürünleri üst üste yerleştirilerek değişiklik yönetimi yapılmıştır.

Anahtar Kelimeler: Spektral İndisler, Otsu eşikleme, Google Earth Engine, Uzaktan Algılama, Sınıflandırma

1.Introduction

Floods are natural events that generally end up as disasters that can negatively affect people and nature. Natural reasons for flooding are raining style, and vegetation change. From a climate change perspective, extreme rains increase while total rain amount decrease (Rozalis et. al, 2010). Unnatural results of flooding may cause from unusual change of nature as agricultural areas and erroneous city plans.

A study (Ceylan, 2007) reports that 29% of the latest disasters in 67 years are floods and inundations. When loss of lives, financial losses, harm to the vegetation is the case, flood modeling is very important. Heavy rains started on 7 January 2020 caused flooding and inundation in downtown and rural agricultural fields. These fields are generally located in the Tarsus district of Mersin city. Mersin city has a history of floods in the years 1957, 1961, 1968, 1973, 1983, 1997, 2001,2007. The longest rain duration was measured as nearly 40 days on 28 Aralık 1968 caused floods in a large area (Bilici and Everest, 2017). Also, a flood was recorded again in the same region on 29 Aralık 2016.

Synthetic-aperture radar (SAR) is a remote sensing system that can run without the magnetic energy of the sun and thermal properties of the world. SAR systems are more preferable to Optical satellite imagery by researchers with the ability to run under all weather conditions, day and night, for flood events. Some research detects floods in city centers with SAR (Mason et. al., 2012, Giustarini et. al., 2012). Also, real-time flood monitoring is available with SAR (Giustarini et. al., 2015).

On SAR images, thresholding is needed to extract the objects (i.e. water, forest, vegetation) from the background. Image thresholding aims to define a threshold by using the intensity levels and applies them to create a binary image. Otsu's (Otsu, 1979) selects the optimal threshold from the image by maximizing between-class variance at the same time minimizing the within-class variance. Some studies have developed the variants of this algorithm by increasing the precision and decreasing the computation time. Wenqing and Jianzhuang (1993) generalized the Otsu algorithm with a 2-dimensional histogram which benefits the pixel-wise gray level information comprises of spatial correlation information from the neighborhood. Zhang and Hu (2008) developed a histogram-based wavelet transform that aims to correct the Otsu threshold and improve the success ratio of image segmentation. Huang et al. (2012) presented a method based on Otsu's algorithm that narrows the range selection of threshold and seeks the optimal threshold.

On the other hand, in remote sensing applications, on RGB imagery, band ratios are used to discover features. Normalized Difference Vegetation Index (NDVI) is the first proposed spectral index that uses Red and near-infrared (NIR) bands, mainly was used for biomass calculation. Normalized Difference Water Index (NDWI) index is proposed by McFeeters (1996) to detect open water areas with Green and NIR bands. Modified NDWI (mNDWI) is obtained by changing the mid-infrared band in the NDWI formula Xu (2006). mNDWI is more advantageous in detecting wetlands in built-up regions. Normalized Difference Moisture Index (NDMI) (Hardisky and Klemas, 1983) is another index which is developed by changing the band Red band in NDVI formula with ShortWave Infrared (SWIR) band.

Our study aims to delineate flooded areas in a region covered mostly with crop fields in the southeast part of Turkey. Sentinel 1 images for the study area are pre-processed with well-known techniques and Otsu (Otsu, 1979) thresholding is applied to obtain the composites regarding the flooded areas. Due to not having the ground truth, spectral indices (Normalized Difference Vegetation Index (NDVI), Normalized Difference Water Index (NDWI), Modified Normalized Difference Water Index (MNDWI), Normalized Difference Moisture Index (NDMI)) are calculated for Sentinel 2 images for the closest dates. The obtained composite is classified with the supervised algorithms. Final Sentinel 1 and Sentinel 2 composites are compared visually to conceptualize the effect of the floods on the study area.

This paper is organized as follows: In Section 2, study area and material information are given. In Section 3, details of the methods are explained. In Section 4, the results of the implementation are provided. Finally, the study is concluded in Section 5.

2. Study Area and Materials

2.1. Study Area

A region in the southeast Mediterranean region of Turkey, east of Mersin province (Also known as Cukurova Region) is selected as the study area. The region is marked with a polygon in GEE named 'mersineast'. Geographical coordinates of the 'mersineast' polygon are given in Table 1.

Table 1. Geographical coordinates of 'mersineast' poligon

Point	Longitude	Latitude
1	34.73552380355155	36.601450257408544
2	35.35075817855155	36.491123379769334
3	35.357624633629676	37.02254331528087
4	34.8591199949578	37.03350686114099
5	34.79045544417655	36.806239043221154
6	34.73552380355155	36.601450257408544

An image taken from GEE which depicts the study area is shown in Figure 1.

Figure 1. GEE image depicting the 'mersineast' polygon

2.2. Materials

Nowadays the bulk of computation and image processing is dependent on local computers and servers. Researchers usually download spatial data from institutions like (European Space Agency) ESA or (United States Geological Survey) USGS and process images by using software like SNAP, QGIS, ArcGIS, etc. In this study we have preferred and used Google Earth Engine (GEE) (Gorelick et al., 2017) cloud computing tool produced by Google Inc. Shortly, GEE provides lots of satellite data (just by importing) with preprocessing tools and classification algorithms. In this study, two different kinds of Remote sensing data are used: Sentinel 1 SAR and Sentinel 2 MSI. Details of the selected satellite data are given in Table 2 with the corresponding dates.

Table 2. Sentinel satellites information used in the study

Satellite System	Dates	Type	Mod	Polarization	Cloud rate
Sentinel-1 SAR GRD: C-band Synthetic Aperture Radar	01.12.2019 - 10.12.2019	Before Event	IW	VV (10m) VH (10m)	-
Sentinel-1 SAR GRD: C-band Synthetic Aperture Radar	07.01.2020 - 09.01.2020	After Event	IW	VV (10m) VH (10m)	-
Sentinel-2 MSI: MultiSpectral Instrument, Level-2A	01.12.2019 - 20.12.2019	Before Event	-	-	<%20
Sentinel-2 MSI: MultiSpectral Instrument, Level-2A	07.01.2020 - 13.01.2020	After Event	-	-	<%20

3. Methods

In this study, Sentinel 1 Radar images are used to delineate flooded areas and Sentinel 2 images are used for the validation of the flooded areas. At first, Sentinel 1 image composite is preprocessed with well-known approaches and the Otsu thresholding method is applied to obtain the final image. On the other side, Sentinel-2 image composite is applied to the spectral indices given in Table 3.

Table 3. Spectral indices applied on Sentinel 2 MSI data

Spectral Index	Usage	Reference
$NDVI = \dfrac{(BAND8 - BAND4)}{(BAND8 + BAND4)}$	Vegetated areas	Rouse et. al. (1974)
$NDWI = \dfrac{(BAND3 - BAND8)}{(BAND3 + BAND8)}$	Flooded areas	McFeeters (1996)
$MNDWI = \dfrac{(BAND3 - BAND11)}{(BAND3 + BAND11)}$	Flooded areas	Xu (2006)
$NDMI = \dfrac{(BAND8 - BAND11)}{(BAND8 + BAND11)}$	Flooded areas	Hardisky and Klemas (1983)

By observing the outputs, the best-performed spectral indices are selected for feature extraction. Features are defined manually for training and validation purposes. Finally, the built-in GEE algorithms Random Forests (Breiman, 2001), Classification And Regression Trees (CART) (Breiman et al., 1984), Support Vector Machines (SVM) (Burges, 1998), and Naive Bayes (Kasif et al., 1998) are used for training and classification. All these processes are given in Figure 2.
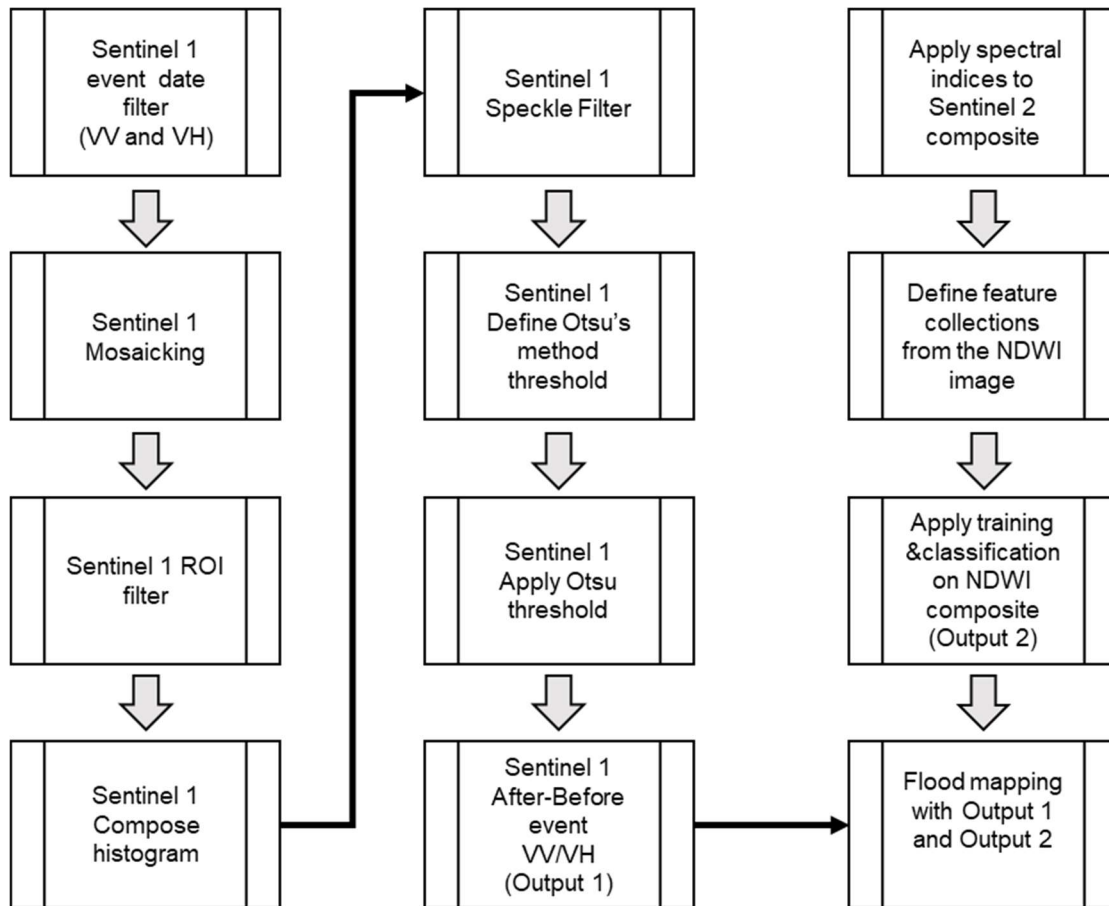
Figure 2. Flowchart of the study

Sentinel 1 dataset is filtered for the given 'before event' and 'after event' dates and mosaicking is applied to obtain the means of the image collections for both VV and VH polarizations. Speckle is a kind of interference caused by rough objects in SAR images. It can be seen as 'salt-and-pepper' appearance and should be reduced for better image interpretation. The obtained composites are again filtered with speckle filter (a kind of smoothing in GEE) to prepare the final products. For both of the composites, histograms are generated and these histograms are used to define the threshold values. Otsu thresholding (Otsu, 1979) is applied to 'before event' and 'after event' composites independently and the differences of these composites are named as 'Output 1' which represents the flooded/inundated areas in the study area. On the other hand, another composite is prepared from Sentinel 2 RGB image for the relevant dates. In the beginning, all the spectral indices given in Table 3 are evaluated and the best performing one is selected for feature preparation. These features are used in the training and validation steps of the classification algorithms. Classification is applied to the composite obtained from the spectral indices and 'Output 2' is obtained. In the end, 'Output 1' and 'Output 2' are evaluated to define the flooded areas of the study area.

GEE provides filtered and processed data of the Sentinel and other satellites. This is advantageous for the researchers and eliminates the burden of preprocessing. Preprocessing steps applied by Google are: Apply orbit file, GRD border noise removal, Thermal noise removal, Radiometric calibration, and Terrain correction.

4. Results

Following the flowchart in Figure 2, a speckle filter is applied to the Sentinel 1 mosaic as a circle with a smoothing radius of 100. The results of this operation for VV polarization are given in Figure 3.
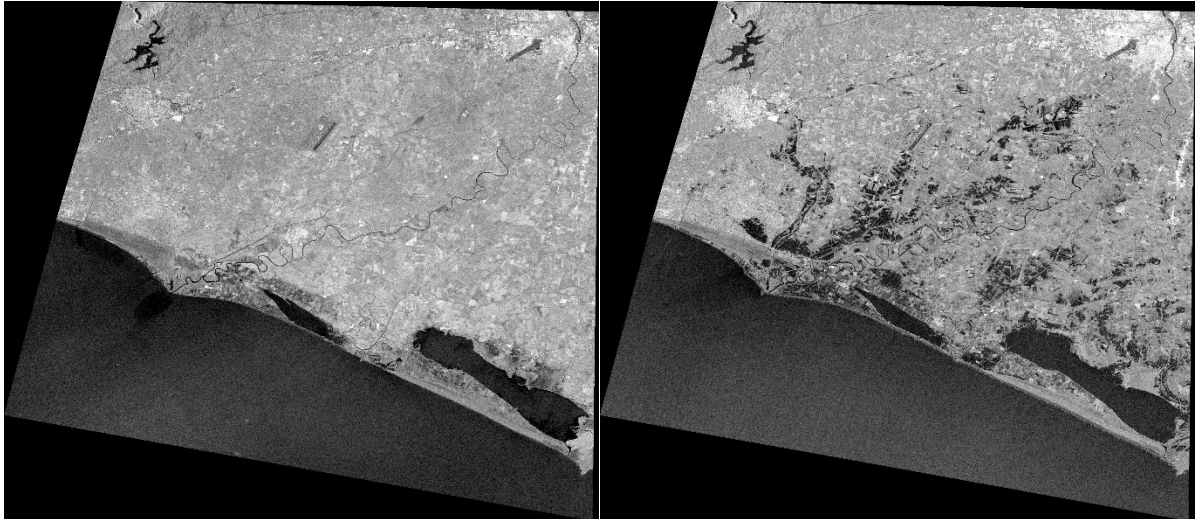
Figure 3. Sentinel 1 image composites after speckle filter for VV polarization, 'before event' (left) 'after event' (right)

In Figure 3, inundated areas can be seen easily and clearly on the right image as black pixels when compared to the image on the left. The resulting image for the application of the speckle filter to the VH polarized image is given in Figure 4.
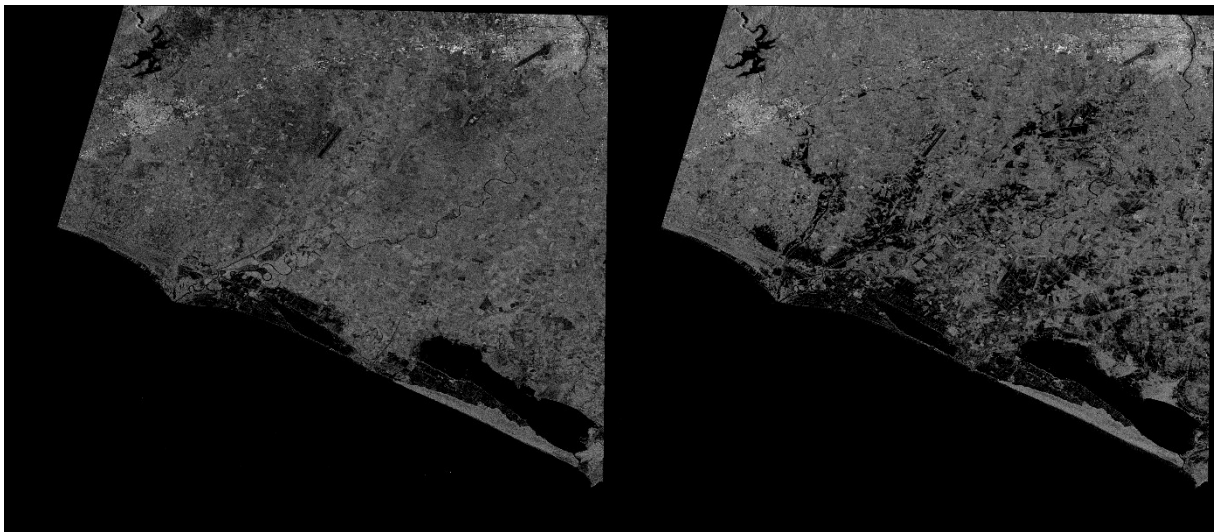

Figure 4. Sentinel 1 image composites after speckle filter for VH polarization, 'before event' (left) 'after event' (right)

In Figure 4, for VH polarization, inundated areas cover broader areas when compared to the VV polarization. But VV polarization composite is more clear and less blurry. Mosaicking and filtering are not always enough to conclude the flood map. To discriminate the features like water, forest, grass, etc. Otsu thresholding is applied to the composites in Figure 3 and Figure 4. Initially, histograms of the four composites are defined and Otsu thresholding is applied independently. Change management is applied by taking the differences of the composites and they are masked by applying Digital Elevation Model (DEM) by eliminating areas with >5% slope value. Finally, the JRC dataset (Pekel et al., 2016) is applied to mask areas with longtime water cover with seasonality >10 months value. Obtained 'after event' outputs after these processes are given in Figure 5 and Figure 6 for VV and VH polarities, respectively.

Figure 5. Sentinel 1 'after event' image composite after Otsu thresholding for VV polarization

In Figure 5 a two-class composite shows the inundated areas are in light gray color. Other areas can be seen in black color.

Figure 6. Sentinel 1 'after event' image composite after Otsu thresholding for VH polarization

In Figure 6, for VH polarization, inundated areas cover fewer areas when compared to the VV polarization. Another map view of these composite masks is given in Figure 7.
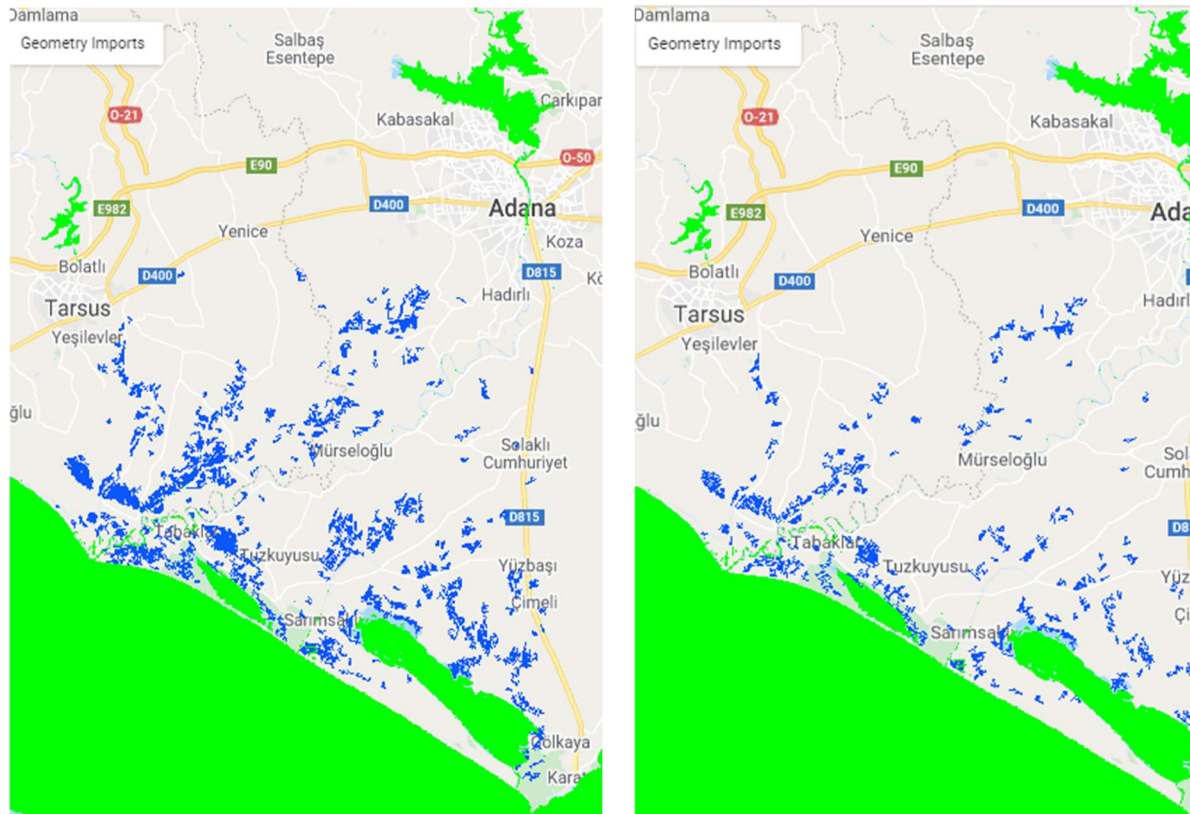

Figure 7. A view of the thresholded Sentinel 1 'after event' image composites for VV (left) VH (right) polarization

Because of the deficiency of ground-truth 'after event' images for the study area, Sentinel 2 'after event' image composites are classified with Random Forests, CART, SVM, and Naive Bayes algorithms. Because of the supervised character of the mentioned algorithms, feature collections are defined from the spectral indice bands of the Sentinel 2 images. At first, all the spectral indices are applied to the Sentinel 2 image composite. Nearly all images show similar results and the clearest one is the NDWI image is selected for feature selection. All features are collected, concerning the 'after event' RGB composite, for both training and validation purposes. The information table for feature collections is given in Table 4.

Table 4. Feature groups collected for both training and validation

Feature collection name	Description	Type	Polygon count
t_open_water	open water	Training	14
t_bare_field	bare field	Training	15
t_forest	forest	Training	11
t_highgreencorp	high green corp	Training	8
v_open_water	open water	Validation	10
v_bare_field	bare field	Validation	10
v_forest	forest	Validation	11
v_highgreencorp	high green corp	Validation	8

In Table 4, it can be seen that four kinds of features are selected as 'open water', 'bare field', 'forest', and 'high green corp'. These features are arbitrarily selected as polygons and it is important to mention that features for training and validation do not coincide. In Table 4, 'Polygon counts' represent the count of each polygon corresponding to each feature. Feature polygons can be seen on the NDWI image given in Figure 7.

Figure 8. Feature polygons are shown on the 'after event' NDWI image composite

Feature collections starting with 't_' in Table 4 are used for the training on 'after event' image composites with Random Forests, CART, SVM, and Naive Bayes algorithms, and classifications are performed accordingly. Gray visualizations of these classifications on NDWI composite image are given in Figure 9.
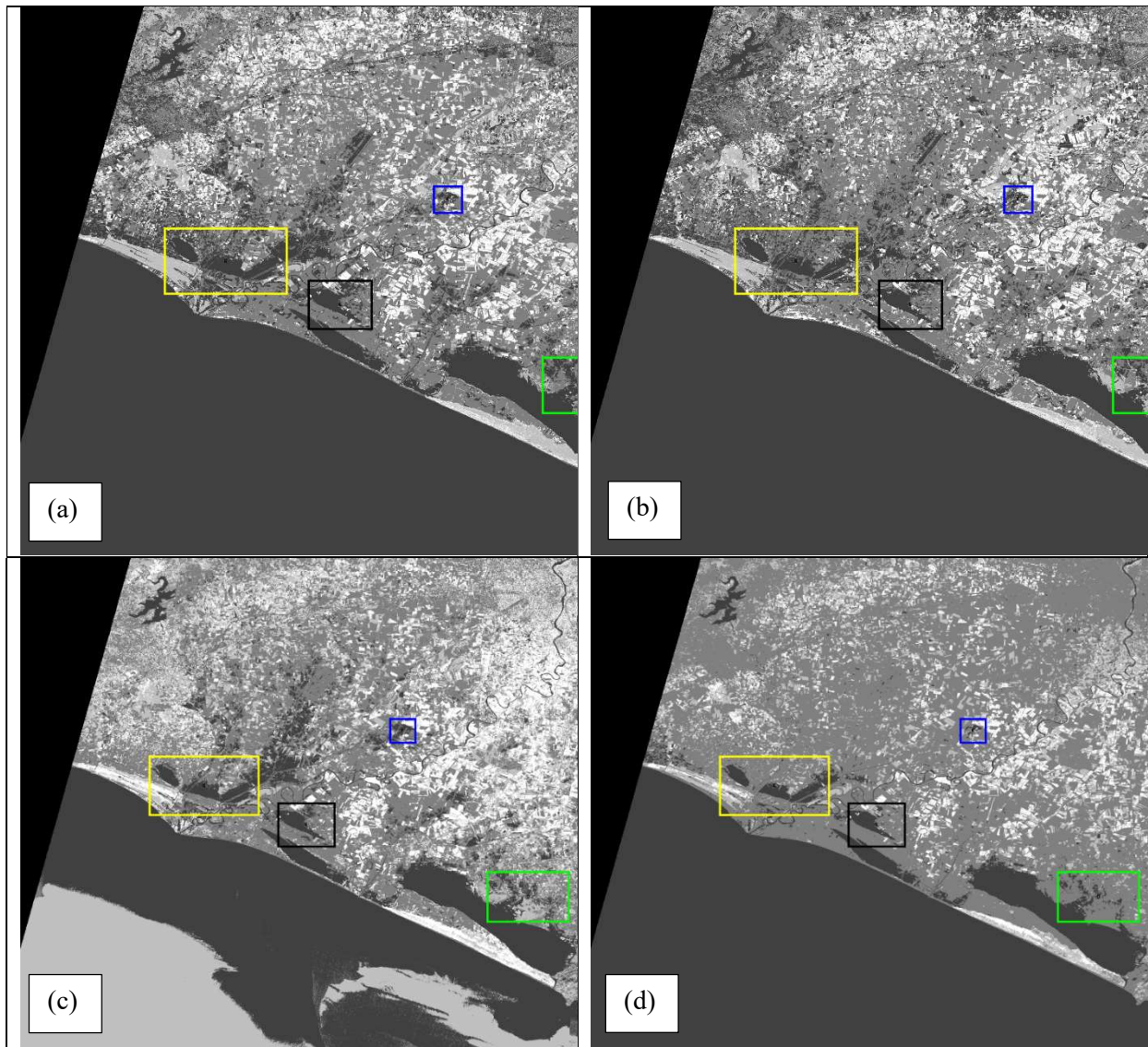
Figure 9. Classification outputs on the NDWI 'after event' image composite (a) Random Forests (b) CART (c) SVM (d) Naive Bayes

As seen in Figure 9, Random Forests, CART, and SVM algorithms show similar open water areas where they can be seen in black areas in the rectangles. These rectangles represent the extremely inundated areas which are interpreted visually. On the other hand, the Naive Bayes algorithm shows a less amount of open water pixels when compared to others. Validation is applied to the classifiers of the algorithms with the validation features given in Table 4 starting with 'v_'. Training and validation accuracy values with corresponding Kappa reliability values of the classification algorithms are given in Table 5.

Table 5. Training and validation accuracy values (%) of the classification algorithms with Kappa values

Classification Algorithm	Training accuracy	Validation accuracy	Kappa value
Random Forests	99.5	99.4	0.988
CART	100	98.0	0.962
SVM	93.2	85.8	0.730
Naive Bayes	85.8	87.5	0.763

Training accuracy values for Random Forests and CART algorithms are very high as seen in Table 5. It is important to observe the validation accuracy values to safely evaluate the training performance. For the before mentioned two algorithms validation values are high as 99.4% and 98% with Kappa reliability values are near to 1 which denotes the consistency with training and validation. On the other hand, the SVM algorithm acquires an acceptable training rate of 93.2% while validation and Kappa values are low as 85.8% and 0.73, respectively. Naive Bayes gives the worst training and validation accuracy values and this can be seen in the image composites.

To compare the final Sentinel 1 flood images (Figure 5 and 6) with the Sentinel 2 classified images Gray outputs of the 'after event' classification images are overlaid with the Sentinel 1 flood images for VV and VH polarizations. These images are given in Figure 10, Figure 11, Figure 12, and Figure 13 for the classified images with Random Forests, CART, SVM, and Naive Bayes algorithms, respectively.

In Figure 10, both images include overlaid flood/inundation images of Sentinel 1 image thresholded with Otsu method (in turquoise color) and Random Forests classification image output (in black color). These two images for VV and VH polarizations are very similar but VV images are more overlaid. When the classification output is examined some black pixel areas do not match with turquoise areas and are shown in yellow rectangles. These areas are known as an airfield (below) and main roads (up). This can be a cause of overfitting of the algorithm or any erroneously prepared feature class.
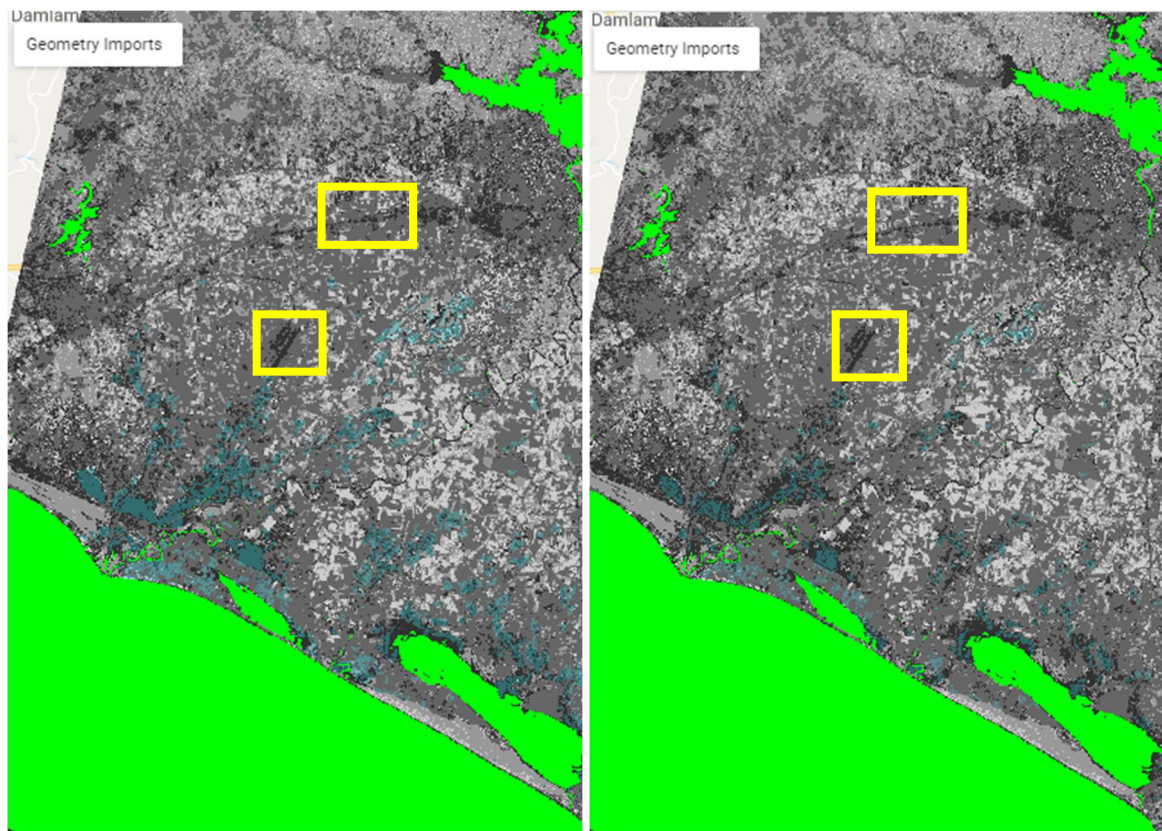

Figure 10. Random Forests classification output overlaid on Sentinel 1 image (left VV- right VH)

In Figure 11, both images of CART classification are visually very similar to the outputs of the Random Forests classifier. This supports the accuracy values given in Table 5.
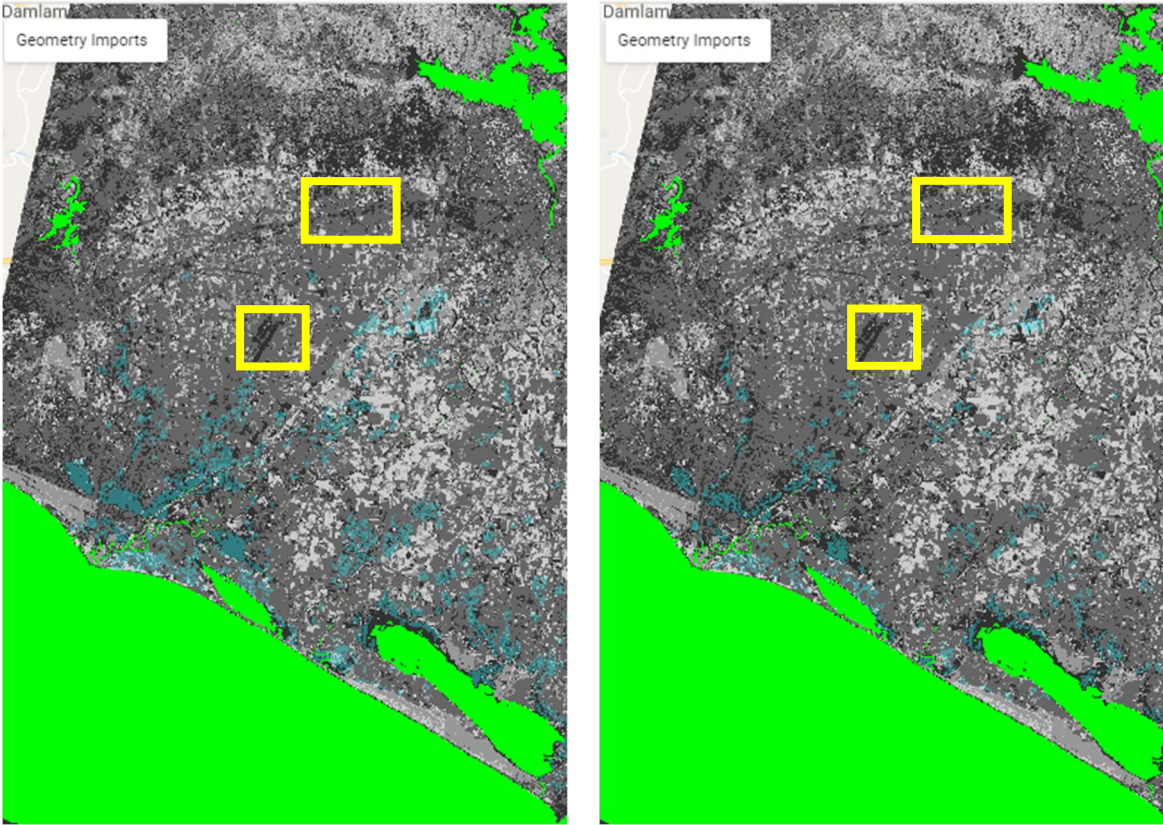
Figure 11. CART classification output overlaid on Sentinel 1 image (left VV- right VH)
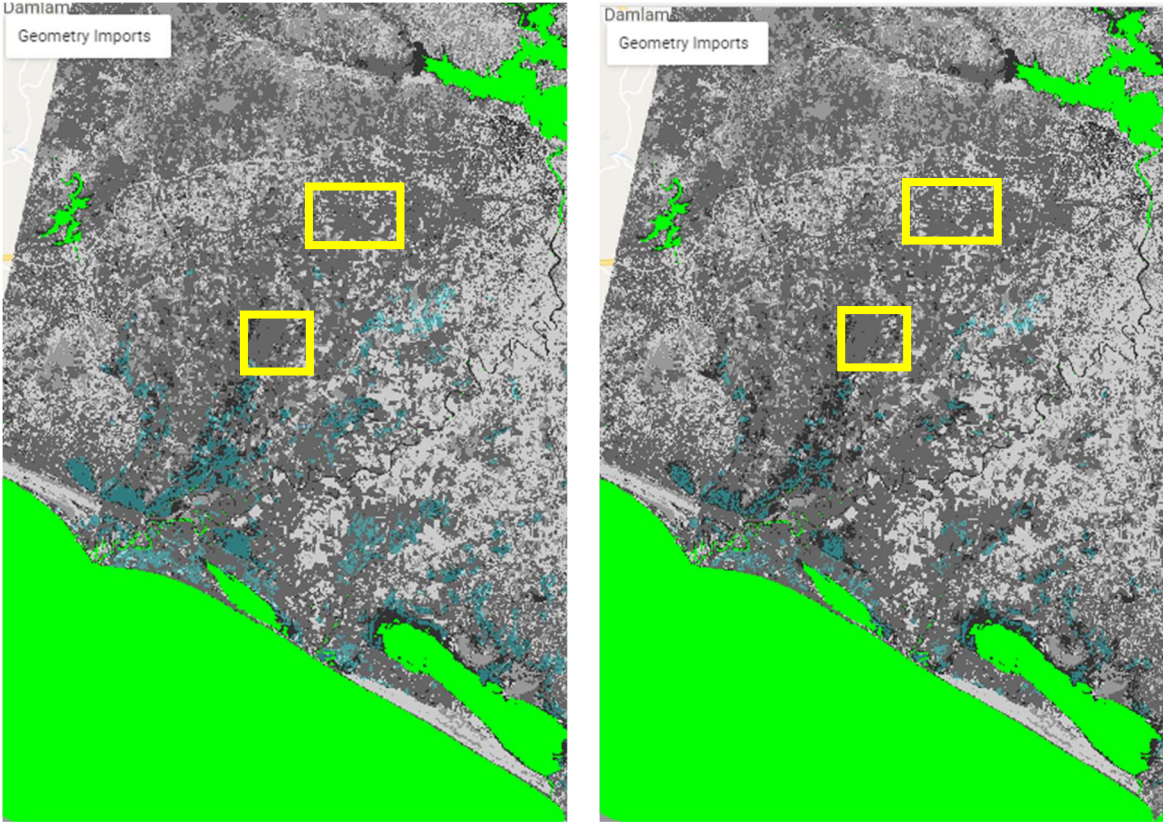

Figure 12. SVM classification output overlaid on Sentinel 1 image (left VV- right VH)

In Figure 12, both images of SVM classification are visually very consistent with the outputs of the Otsu thresholded Sentinel 1 image. But generally, Random Forests and CART output images provide better classifier output. Surprisingly the built-up areas in yellow squares seem very little inundated.
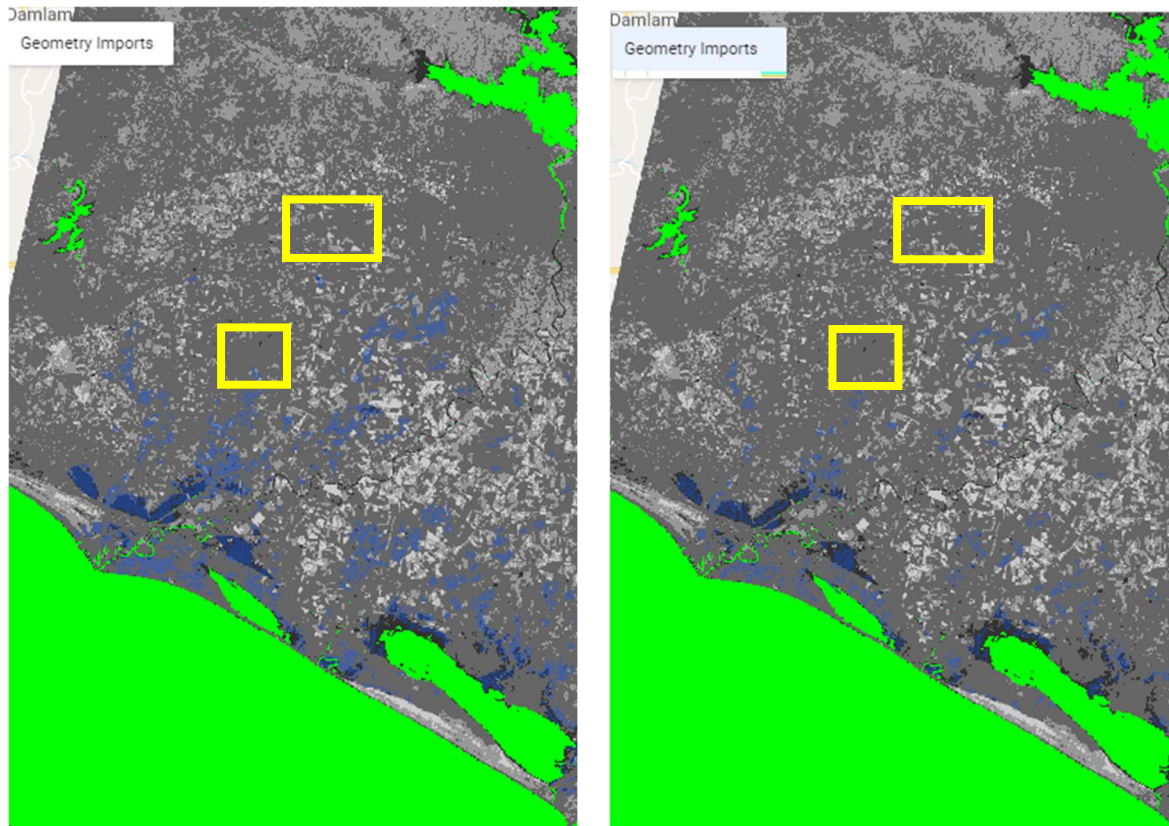

Figure 13. Naive Bayes classification output overlaid on Sentinel 1 image (left VV- right VH)

In Figure 13, dark blue pixels represent overlaid areas and light blue areas inundated areas, respectively. Overlaid areas produced by the Naive Bayes algorithm are very little when compared to the other applied algorithms.

5. Conclusions

In this study, we have used Sentinel-1 satellite Radar imagery with the Otsu thresholding method to identify the flooded areas in the Tarsus district of Mersin, Turkey. Mersin city has a long history of floods and we have investigated the most recent event in January 2020.

In the study, Sentinel-2 imagery supported the Sentinel-1 outputs with a classification process. Four spectral indices are applied to the Sentinel-2 composite for the nearest dates after the flood event. Visually, all indices provided near results. NDWI composite, which is the least blurry one is selected for feature generation. By using this composite training and validation feature collections are prepared. Four well-known classification algorithms (Random Forests, CART, SVM, and Naive Bayes) are selected to train the image model. While training and validation values are high for Random Forests and CART algorithms, Random Forests algorithm provide better accuracy and output composites of Random Forests algorithm generally overlay with the obtained Sentinel-1 flood map.

Obtained results show that, flooded areas were generally clustered around 'Seyhan' river where it ends in the Mediterranean Sea. But the floods were not limited in the Tarsus Plain. Also, the neighboring Çukurova Plain was negatively affected by floods covering the agricultural plain fields on the north of 'Tuz' and 'Akyatan' lakes.

This study is one of the implementations of the hybrid usage of Radar and Optical imagery together for flood disasters. Optical imagery can be used to verify the flood mapping provided by Sentinel-1 or other Radar imagery, when ground truth for the study area is unavailable.

Acknowledgments

Conflicts of Interest

The authors declare no conflict of interest.

References

Bilici, Ö. E., Everest, A., 2017. 29 Aralik 2016 Mersin Selinin Meteorolojik Analizi Ve İklim Değişikliği Bağlantisi. Eastern Geographical Review, 22(38).

Breiman, L., 2001. Random forests. Machine learning, 45(1), 5-32.

Breiman, L., Friedman, J., Stone, C. J., Olshen, R. A., 1984. Classification and regression trees. CRC press.

Burges, C. J., 1998. A tutorial on support vector machines for pattern recognition. Data mining and knowledge discovery, 2(2), 121-167.

Ceylan, A., Kömüşcü, A. Ü., 2007. Meteorolojik karakterli doğal afetlerin uzun yıllar ve mevsimsel dağılımları. İklim Değişikliği ve Çevre, 1(1), 1-10.

Giustarini, L., Vernieuwe, H., Verwaeren, J., Chini, M., Hostache, R., Matgen, P., De Baets, B., 2015. Accounting for image uncertainty in SAR-based flood mapping. International journal of applied earth observation and geoinformation, 34, 70-77.

Giustarini, L., Hostache, R., Matgen, P., Schumann, G. J. P., Bates, P. D., Mason, D. C., 2012. A change detection approach to flood mapping in urban areas using TerraSAR-X. IEEE transactions on Geoscience and Remote Sensing, 51(4), 2417-2430.

Gorelick, N., Hancher, M., Dixon, M., Ilyushchenko, S., Thau, D., Moore, R., 2017. Google Earth Engine: Planetary-scale geospatial analysis for everyone. Remote Sensing of Environment.

Hardisky, M. A., Klemas, V., Smart, M., 1983. The influence of soil salinity, growth form, and leaf moisture on the spectral radiance of. Spartina alterniflora, 49, 77-83.

Huang, M., Yu, W., Zhu, D., 2012 August. An improved image segmentation algorithm based on the Otsu method. In 2012 13th ACIS International Conference on Software Engineering, Artificial Intelligence, Networking and Parallel/Distributed Computing (pp. 135-139). IEEE.

Kasif, S., Salzberg, S., Waltz, D., Rachlin, J., Aha, D. W., 1998. A probabilistic framework for memory-based reasoning. Artificial Intelligence, 104(1/2), 297–312

Mason, D. C., Davenport, I. J., Neal, J. C., Schumann, G. J. P., Bates, P. D., 2012. Near real-time flood detection in urban and rural areas using high-resolution synthetic aperture radar images. IEEE transactions on Geoscience and Remote Sensing, 50(8), 3041-3052.

McFeeters, S. K., 1996. The use of the Normalized Difference Water Index (NDWI) in the delineation of open water features. International journal of remote sensing, 17(7), 1425-1432.

Otsu, N., 1979. A threshold selection method from gray-level histograms. IEEE transactions on systems, man, and cybernetics, 9(1), 62-66.

Pekel, J. F., Cottam, A., Gorelick, N., Belward, A. S., 2016. High-resolution mapping of global surface water and its long-term changes. Nature, 540(7633), 418-422.

Rozalis, S., Morin, E., Yair, Y., Price, C., 2010. Flash flood prediction using an uncalibrated hydrological model and radar rainfall data in a Mediterranean watershed under changing hydrological conditions. Journal of hydrology, 394(1-2), 245-255.

Rouse, J. W., Haas, R. H., Schell, J. A., Deering, D. W., 1974. Monitoring vegetation systems in the Great Plains with ERTS. NASA special publication, 351(1974), 309.

Xu, H., 2006. Modification of normalised difference water index (NDWI) to enhance open water features in remotely sensed imagery. International journal of remote sensing, 27(14), 3025-3033.

Wenqing, L. J. L., Jianzhuang, L., 1993. The Automatic thresholding of gray-level pictures via two-dimensional otsu method [J]. Acta Automatica Sinica, 1, 015.

Zhang, J., Hu, J., 2008 December. Image segmentation based on 2D Otsu method with histogram analysis. In 2008 international conference on computer science and software engineering (Vol. 6, pp. 105-108). IEEE.